Nano Research
DOI 10.1007/s12274-013-0319-5
Research Article
ISSN 1998-0124
CN 11-5974/O4

Substrate-based galvanic replacement reactions carried out on heteroepitaxially formed silver templates

Kyle D. Gilroy[1], Pouyan Farzinpour[1], Aarthi Sundar[1], Teng Tan[2], Robert A. Hughes[1] (✉), and Svetlana Neretina[1] (✉)

[1] *College of Engineering, Temple University, Philadelphia 19122, USA*
[2] *Department of Physics, Temple University, Philadelphia 19122, USA*

Received: 11 March 2013
Revised: 11 April 2013
Accepted: 12 April 2013

KEYWORDS

galvanic replacement,
heteroepitaxy,
nanohut,
nanobowl,
semishell,
plasmon

ABSTRACT

Galvanic replacement reactions have been widely used to transform solution dispersed silver template structures into intricate nanoshell geometries. Here, we report on the use of these same reactions to form hollow substrate-supported Au–Ag nanoshells from silver templates having a heteroepitaxial relationship with the underlying single crystal substrate. The structures obtained exhibit a nanohut geometry, show highly tunable plasmonic properties and are formed as periodic arrays using a lithography-free technique. When removed from the substrate the inverted nanohuts appear as nanobowls with a notch in the rim. The study lays the groundwork for wafer-based devices utilizing nanoshells located at site-specific locations.

1 Introduction

Progress directed toward the application of noble metal nanostructures [1–4] has been reliant on the establishment of facile synthetic protocols [5–7] able to tailor the plasmonic response to meet the demands of specific applications. Breakthroughs have increasingly relied on synthetic strategies yielding complex geometries with asymmetric, core-shell or hollowed morphologies [8–12]. In this regard, galvanic replacement reactions [13–15] offer pathways toward the formation of intricate nanostructures using synthetically simple reactions where complex products are derived from preformed templates. These reactions are reliant on solution-based oxidation–reduction reactions which occur when atoms of a solid metal (i.e., the template) spontaneously react with ions of a second metal having a higher electrochemical potential. The ensuing reaction results in the simultaneous heteroepitaxial deposition of the second metal onto the template as the template material is steadily dissolved into the solution. With both deposition and dissolution

Address correspondence to Robert A. Hughes, hughesr@temple.edu; Svetlana Neretina, neretina@temple.edu

being highly dependent upon the crystallographic orientation and faceting of the template, complex nanostructures can be engineered through the use of appropriate templates which are reacted to the desired endpoint. Such reactions typically lead to the formation of hollow nanoshells which exhibit highly tunable plasmonic properties due to coupling between plasmons formed on the inner and outer surfaces of the structure [16]. Also of significance is the strong sensitivity of the position of the localized surface plasmon resonance (LSPR) to changes in the index of refraction of the adjacent medium [17, 18]. Together these properties make nanoshells candidate materials for use in biomedical [15, 19], sensor [10, 17, 18, 20] and catalytic applications [21, 22].

Galvanic replacement reactions have been extensively studied for the case of template structures dispersed in solution. Few investigations, however, have been carried out on substrate-immobilized templates. Notable studies include the use of replacement reactions for: (i) the deposition of nanostructured gold on nickel electrodes for mercury vapor sensing [23], (ii) the preparation of nanoporous copper surfaces on nickel foils for catalytic applications [24], (iii) the formation of chemically stable surface enhanced Raman spectroscopy (SERS) active surfaces on glass substrates though the replacement of vertically aligned silver nanorods with gold [25], (iv) the replacement of electrochemically synthesized iron nanocubes on carbon with gold and palladium [26], and (v) the epitaxial growth of smooth copper films on (111)-oriented single crystals of gold and silver using sacrificial lead films as a template material [27]. While these studies have demonstrated the viability of substrate-based galvanic replacement reactions, they have not fully taken advantage of unique capabilities accessible through the use of nanostructured templates. Specific advantages include the placement of templates at site-specific locations and having them heteroepitaxially aligned with the underlying substrate. Fully exploiting these capabilities could result in the synthesis of substrate-based periodic arrays of aligned crystalline nanostructures with a high degree of complexity, tunability and functionality. Here, we report on the galvanic replacement of heteroepitaxially aligned nanostructured silver templates formed on (0001)-oriented sapphire substrates. Reported is the synthesis and characterization of substrate-immobilized Au–Ag nanohut structures formed as both periodic arrays and as structures with randomized size and placement.

2 Experimental

Substrate-based silver templates were assembled on (0001)-oriented sapphire substrates as both randomly positioned structures with a substantial size distribution and as periodic arrays with a narrow size distribution. The procedure for forming the random structures [28] (Fig. 1(a)) involves the sequential deposition of a sacrificial antimony layer and an ultrathin silver film. When heated, the layered structure results in the agglomeration of silver to form nanostructures (Fig. 1(c)), but where the concurrent sublimation of antimony results in nanostructures which have a higher degree of shape uniformity than similarly sized structures formed in the absence of antimony (see Fig. S1 in the Electronic Supplementary Material (ESM)). The assembly route also allows for the formation of silver templates over the large areas required for optical and structural characterization. Through adjustments to the antimony and silver layer thickness both large (diameter < 250 nm) and small (diameter < 50 nm) silver templates were fabricated.

The arrayed silver templates were produced using dynamic templating [29] (Fig. 1(b)), a lithography-free processing route similar to that used for the non-arrayed structures, but where a periodicity is imposed on the assembly process through the use of a shadow mask. It involved the deposition of 70 nm of antimony followed by 5 nm of silver through a shadow mask with 1.2 μm diameter openings separated by a center-to-center distance of 2.6 μm. Removal of the shadow mask yields silver-topped antimony pedestals. When heated, the antimony preferentially sublimes from the sides of the pedestal causing the areal dimensions of the pedestal, on which silver is agglomerating, to rapidly shrink. This leads to a forced migration of silver to the center of each pedestal, where the rate and areal extent over which the agglomeration occurs exceeds by orders of magnitude that of a silver pedestal deposited directly on the substrate surface. At the

end of the process, the antimony has completely sublimed leaving behind a periodic array of substrate-immobilized silver nanostructures with diameters of 250 nm (Fig. 1(d)). These silver templates, while having the disadvantage of low areal coverage (area = 3 mm^2, density = 1.5 × $10^7/cm^2$), were advantageous in that they exhibited a high degree of size uniformity and could be formed as periodic arrays.

Galvanic replacement reactions (Fig. 1(e)) on the silver template structures were carried out using a synthetic protocol similar to that devised by Xia and co-workers [13]. Briefly, a three-neck flask was filled with an aqueous $HAuCl_4$ solution (10 mL) and the contents refluxed for 10 min. The concentration for preparing the larger templates (diameter < 250 nm) was varied from 10 to 100 μM for both the arrayed and non-arrayed configurations. For smaller templates (diameter < 50 nm), lower concentrations were used (0.5–2 μM) since five times less silver was deposited on the substrate surface. The substrate was then immersed into the $HAuCl_4$ solution for 10 min, after which it was slowly pulled out and dried in a flow of argon gas. It should be noted that the exposure of the silver template structures to air was minimized either by reacting them immediately following assembly or storing them in a 1 × 10^{-6} Torr vacuum environment.

3 Results and discussion

Figures 2(a) and 2(b) show tilted- and top-view scanning electron microscopy (SEM) images of unreacted templates and those exposed to 10 and 100 μM aqueous $HAuCl_4$ for both the non-arrayed and arrayed configurations. Prior to reaction the silver templates exhibit a morphology characteristic of a droplet in contact with a surface, but where significant faceting is observed. The shape is typical for high surface energy metals that have agglomerated on a low surface energy substrate [30, 31]. Also noteworthy, is that, unlike solution-based synthesis routes, the templates are free of capping agents. As the templates are reacted they undergo a morphological transformation

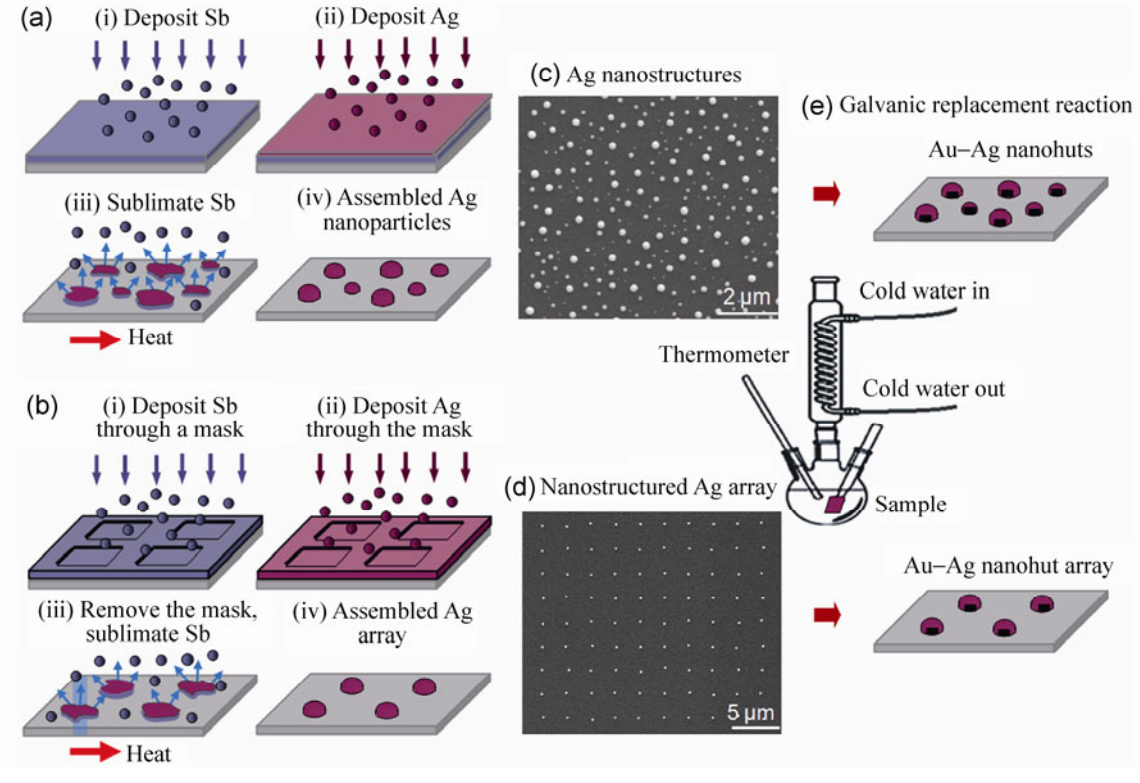

Figure 1 Schematics showing the synthetic routes used to assemble (a) non-arrayed and (b) arrayed silver nanostructures. The SEM images show structures with (c) a substantial size distribution situated at random locations and (d) arrayed structures with a narrow size distribution. Both structures were used as templates in (e) galvanic replacement reactions yielding substrate-immobilized Au–Ag nanohuts.

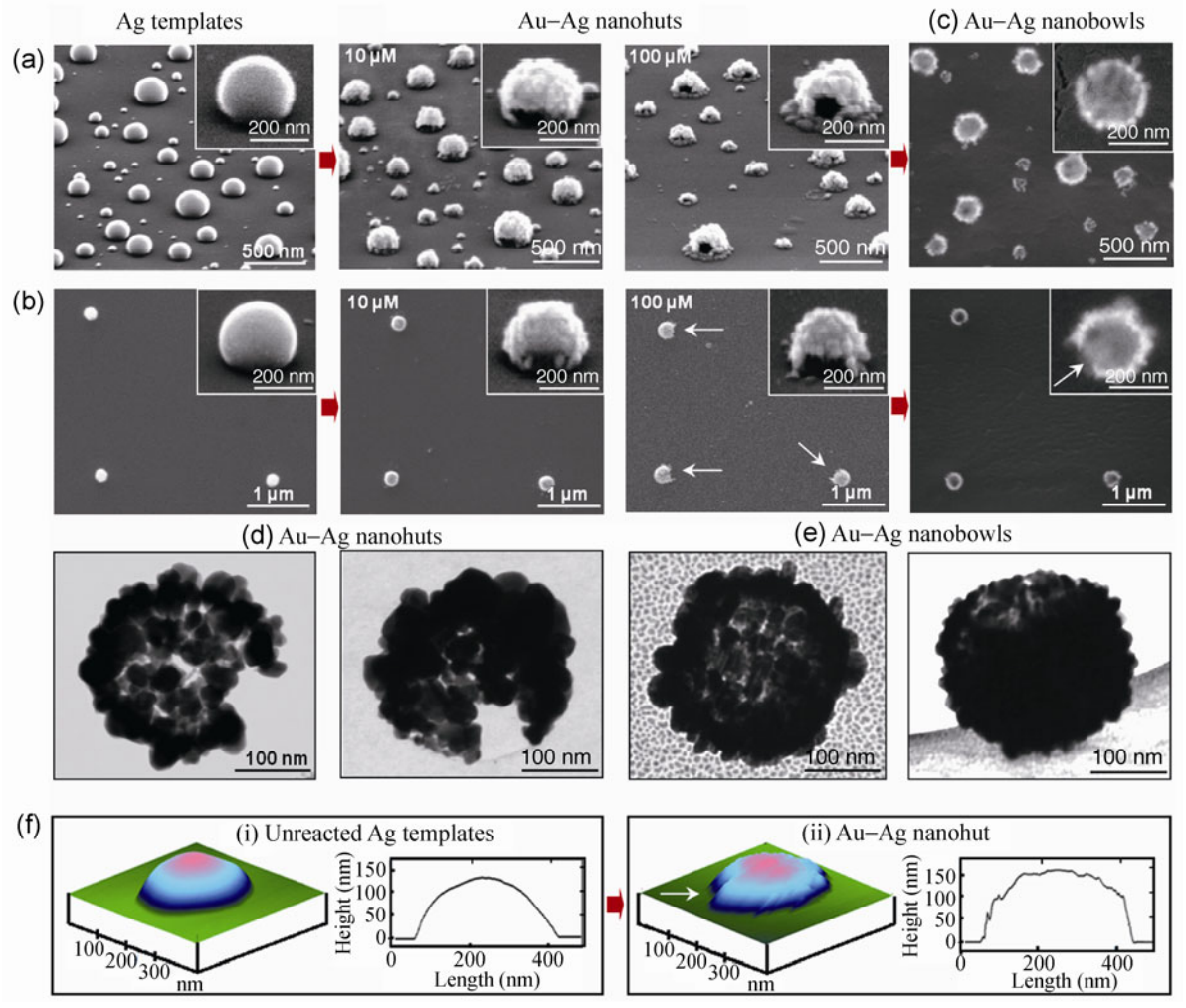

Figure 2 SEM images showing the morphology of unreacted templates and nanohuts formed through galvanic replacement reactions using 10 and 100 μM solutions in the (a) non-arrayed and (b) arrayed configurations. (c) Images of non-arrayed and arrayed nanohut structures which have been removed from the sapphire substrate using Scotch tape. Note that the inverted structures appear as nanobowls where the rim shape has been influenced by the six-fold faceting associated with the initial template structure. The tilt angle for all insets is 65°. (d) Top- and tilted-view TEM images of nanohuts assembled directly on Si_3N_4 support films. (e) Top- and titled-view TEM images of nanobowls removed from sapphire substrates. (f) AFM image and the associated cross-section for an individual template and the same structure after it has been 75% reacted to form a nanohut. Note that the height of the structure has increased from 135 to 158 nm. The white arrows on both the SEM and AFM images point toward the single side opening found on each nanohut.

to a "nanohut" geometry which results in (i) a roughening of the surface, (ii) a hollowing of the interior, and (iii) the appearance of an opening at the base of the structure. The non-arrayed samples (Fig. 2(a)) exhibit structures in various stages of the reaction since smaller structures have less material to react than larger ones. For the 10 μM sample the opening takes on a rectangular geometry. For the 100 μM sample the opening appears partially closed and a ring of porous gold encircles the structure at its base. In contrast, the arrayed templates, when reacted (Fig. 2(b)), show a high degree of uniformity and evolve at a slower rate. The top-view SEM image for the unreacted arrayed templates show faceted structures with uniform contrast as is expected for solid particles. Conversely, arrayed templates reacted using the 10 μM and 100 μM concentrations show significant contrast, exhibiting a dark inner circle surrounded by a bright

outer ring. Such a pattern is characteristic of hollow structures [32]. Also apparent from the SEM image for the 100 μM sample is that each arrayed structure has a large single opening on its side. Fully reacted nanohut structures in both the arrayed and non-arrayed configurations were easily removed from the substrate using Scotch tape. SEM images of the tape (Fig. 2(c)), show intact structures which, because they are now inverted, appear as nanobowls with a notch in the rim. TEM images of nanohuts assembled directly on Si_3N_4 support films (Fig. 2(d)) as well as individual nanobowls removed from the sapphire substrate (Fig. 2(e)) confirm the hollow geometry and show features consistent with structures derived from faceted templates. It should be noted that both the arrayed nanohuts and nanobowls could be produced over large areas (see Fig. S2 in the ESM).

Through the use of substrate alignment markers it was also possible to measure the height of an individual template structure using an atomic force microscope (AFM), react the template and then return to the identical location to measure the height of the nanohut formed. The composition of the reacted structure was then measured using energy dispersive spectroscopy (EDS). Figure 2(f) shows AFM images and the associated cross-sections for a structure which has undergone 75% replacement. The height of the structure increased by 17%, a value somewhat larger than the 12.4% value derived for the expected growth mode which sees a hollowing of the template as gold is deposited uniformly on its outer surface in a 3:1 Ag:Au replacement ratio [15, 18, 25]. The larger than expected value likely indicates the preferential attachment of material to the top of the structure. While the AFM cross-section suggests that this is indeed the case, the conclusion is somewhat obfuscated by the fact that the measured values are a convolution of the probe geometry and the surface features being measured, the result of which is an exaggerated structure width.

θ–2θ X-ray diffraction (XRD), a technique sensitive to periodicities perpendicular to the surface of the substrate, was carried out on the non-arrayed templates and identical templates exposed to the galvanic replacement reaction. The diffraction pattern for the silver templates (Fig. 3(a)) indicates that the [110]-orientation is preferred, but where small quantities of the [100]-orientation also exist. For the dominant orientation, the [110]-direction is perpendicular to the surface of the substrate while the [001]-, [00$\bar{1}$]-, [$\bar{1}$,1,1]-, [$\bar{1}\bar{1}$1]-, [1$\bar{1}$1]- and [1$\bar{1}\bar{1}$]-directions are parallel as is depicted by the Wulff shape shown schematically in Fig. 3(a). With gold and silver sharing the same face-centered-cubic (fcc) crystal structure and having nearly the same lattice constant (Ag: a = 4.085 Å, Au: a = 4.078 Å) the peak positions are not expected to change appreciably after the replacement reaction occurs. New peaks are also not expected provided that the gold deposits on the template in a heteroepitaxial manner. Figure 3(b) confirms these expectations for the large ensemble of nanostructures probed in the XRD measurement, only showing reflections at the

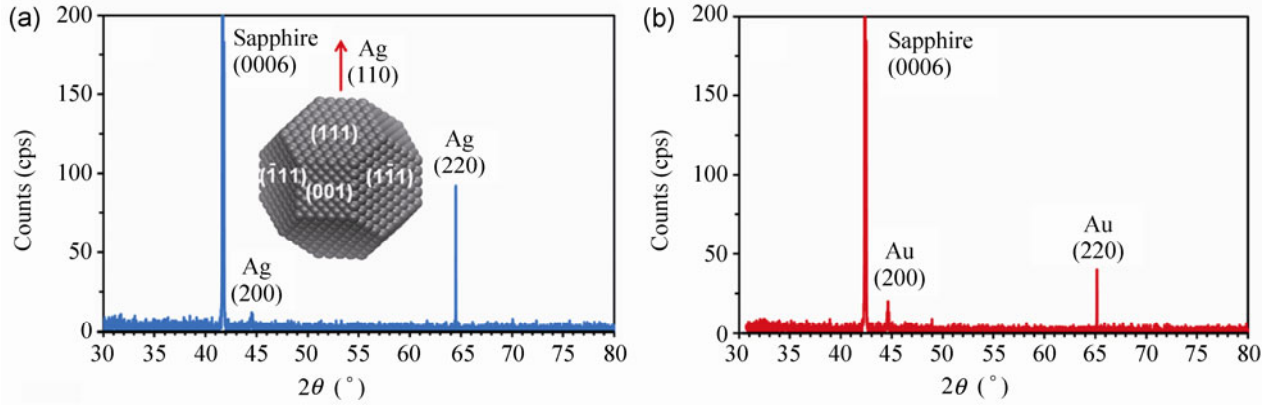

Figure 3 θ–2θ X-ray diffraction scans for (a) the non-arrayed silver templates and (b) an identical sample after 80% of the silver has been replaced with gold to form nanohut structures. The inset shows a schematic of a [110]-oriented Wulff shape which depicts the underlying crystallography as it relates to the {001}- and {111}-planes.

same 2θ values.

Figure 4 shows the extinction spectra for non-arrayed silver templates with an average diameter of 30 nm reacted to varying degrees. The measurements were taken using unpolarized light where the ***E***-field and propagation direction (***k***) are parallel and perpendicular to the substrate surface, respectively. Observed is a substantial broadening of the LSPR peak as it red-shifts from 436 nm for the non-reacted templates to 745 nm for the fully reacted structures. The accompanying color change observed in reflectance is shown in the inset to Fig. 4. This ability to tune the plasmonic response over such a large range starting from identical templates is one of the key advantages of galvanic replacement reactions [33]. Of significance is the fact that the nanohut is a highly asymmetric due to both its hemispherical-like geometry and the presence of the rectangular opening at its base. This places the nanohut in a class of symmetry breaking structures (e.g., semishells [10, 34–37], nanobowls [38–41], and nanocrescents [42, 43]) which offer polarization dependent plasmon modes with large local field enhancements and a high degree of tunability.

Simulations using the discrete dipole approximation (DDA) [44] were carried out to examine the influence of both the opening and substrate on the nanohut extinction spectra. Figure 5 shows the spectra

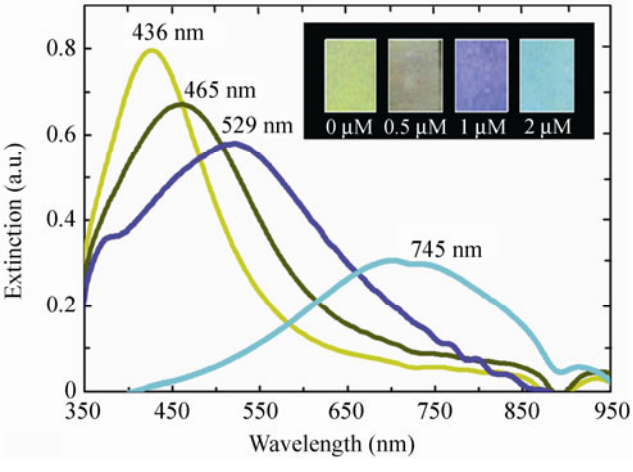

Figure 4 The extinction spectra for non-arrayed silver templates with an average particle size of 30 nm exposed to various $HAuCl_4$ concentrations. Concentrations of 0, 0.5, 1 and 2 μM yield LSPR peaks at 436, 465, 529 and 745 nm, respectively. The inset shows optical images of the samples taken in reflectance.

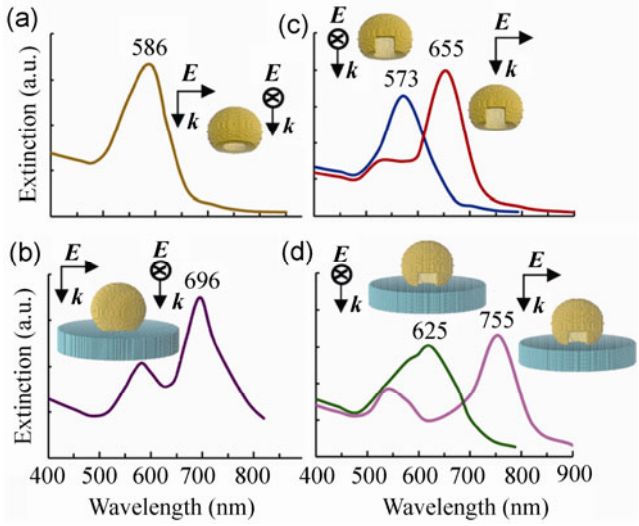

Figure 5 Calculated extinction spectra of (a) a hollow gold shell and the same shell (b) resting on a sapphire substrate, (c) with a rectangular side opening and (d) resting on a substrate and having rectangular side opening. The shell is a truncated sphere (diameter = 40 nm, shell thickness = 5 nm) which forms a 130° contact angle with the substrate. The side opening is 10 nm in the vertical direction and 14 nm in the horizontal direction. The substrate has a diameter of 80 nm and thickness of 15 nm. The incident light is transversely polarized (i.e., the ***E***-field is parallel to the substrate). For the nanohut geometry, spectra are calculated using transverse ***E***-fields that are both through and parallel to the side opening.

for free-standing gold structures with and without side openings and those same structures supported by a sapphire substrate. Transverse ***E***-fields in the absence of a side opening give rise to a polarization independent response yielding a LSPR peak at 586 nm for the freestanding structure (Fig. 5(a)). The break in symmetry resulting from the introduction of a side opening into this structure results in a strong polarization dependence with ***E***-fields through and parallel to the opening yielding resonances at 573 and 655 nm, respectively (Fig. 5(c)). It is noted that this behavior is qualitatively similar to the simulated and experimental results obtained for semishells with a perforation which intersects the edge of the shell [45]. The inclusion of a supporting substrate into the simulation (Figs. 5(b) and 5(d)) leads to a strong red-shift in the LSPR peaks and the establishment of a high energy quadrupolar mode. With red-shifts of 52 and 100 nm for ***E***-fields through and parallel to the side opening, the substrate acts to substantially increase the degree of optical

anisotropy. Because the fabricated nanohuts used in the current study had side openings in numerous directions, direct comparisons between simulation and experiment remain challenging. However, upon recognizing that the experimental data is an average over all transverse polarizations, the simulations are consistent with the large red-shift and substantial broadening in the LSPR peak observed for the fully reacted structures.

This initial investigation into the use of heteroepitaxially defined structures as templates for galvanic replacement reactions demonstrates the ability to fabricate substrate-based nanoshell structures, place them at site-specific locations and obtain a tunable LSPR peak. In general, the replacement reaction proceeds in much the same manner as it does for solution-based templates. Au^{3+} ions react with the template forming a shell which has a heteroepitaxial relationship with underlying silver. Coinciding with the gold deposition is Au–Ag alloying as well as the loss of template material to the solution in the form of Ag^{+} ions, a process facilitated by the appearance of a hole in the shell that allows these ions to emerge and which exposes both the gold shell cathode and the silver template anode to the aqueous solution. The latter stages of the reaction are characterized by a dealloying process which leads to both a weakening of the shell and fragmentation [46]. In time, the silver template is exhausted and the galvanic replacement reaction terminates. While similarities exist, a number of unique characteristics are observed. Foremost, is the fact that the nanohut structures exhibit a unique geometry. The rigid substrate, for example, encloses one side of the nanoshell, the result of which is a structure with increased mechanical robustness and an LSPR peak which is red-shifted due to interactions between the plasmon resonance and the dielectric environment of the substrate. The structures also exhibit a single large rectangular opening at their base instead of the many small openings typically observed for fully reacted solution-based templates.

The mechanisms guiding the shape and placement of the shell opening are expected to originate from surface energy considerations associated with both template formation and the galvanic replacement process. Template formation is driven by the fact that a high surface energy metal is agglomerating on a low surface energy substrate. For this scenario, the final template shape results from the interplay between numerous factors [31]. Foremost, are those which tend to reduce the overall surface energy, the most important of which are (i) the formation of energetically favorable facets, (ii) a lowering of the surface-area-to-volume ratio and (iii) the establishment of an optimum contact angle with the substrate. For the fcc crystal structure of silver the hierarchy in surface energies (i.e., $\gamma\{110\}>\gamma\{001\}>\gamma\{111\}$) [47] tends toward the establishment of faceting consistent with the Wulff shape [31] (i.e., a truncated octahedron containing eight hexagonal {111}-facets and six square {001}-facets). Structures with this exact shape, however, are not typically observed as high processing temperatures and nanoscale particle dimensions lead to a structure which is more rounded while substrate–template surface energy considerations result in a further truncation of the Wulff shape in a plane parallel to the surface of the substrate [31]. Other factors of significance include the presence of impurities, interface strain, defects and the processing conditions. Nevertheless, features associated with an underlying Wulff shape, rounded corners and substrate truncation are all observed in SEM images of the silver templates. Of particular note, however, is that the top-view SEM images exhibit a near-hexagonal shape which is consistent with a [110]-oriented Wulff-like geometry and the corresponding [001], [00$\bar{1}$], [$\bar{1}$,1,1], [$\bar{1}\bar{1}$1], [1$\bar{1}$1] and [1$\bar{1}\bar{1}$] side facets. When these templates are reacted, the galvanic replacement process will initiate at sites with relatively high surface energies. Such sites include high surface energy facets, high curvature points where facets intersect and defect structures [32]. Candidate sites at the base of the structure include (i) the aforementioned high surface energy [001]- and [00$\bar{1}$]-facets, (ii) the intersection points between the six side facets, and/or (iii) the dislocation defects caused by the lattice mismatch between the silver template and the underlying substrate [48]. It is also noted that both the size of the template and its opening are considerably larger than is typical for galvanic replacement reactions. With this opening being the primary route from which silver exits the interior of the structure, the resulting Ag^{+} ion flux is likely to

have a strong local influence on solution kinetics.

While this investigation only focused on a particular substrate-based galvanic replacement reaction, it should be recognized that numerous future possibilities exist in terms of the nanomaterials accessible, in obtaining a fundamental understanding of the underlying mechanisms and in using these structures to advance substrate-based device applications. In particular, the heteroepitaxial relationship between the template structure and the underlying substrate provides the means to alter the template orientation, shape and faceting through variations to the substrate material, its crystallographic orientation, the lattice mismatch and surface reconstructions [31, 49, 50]. This variability, in combination with the facet selective nature of the replacement process, provides the, as of yet, unexplored opportunity to shape-engineer substrate-based nanoshell structures. Substrate-immobilized templates also offer an excellent platform for advancing the understanding of the underlying mechanisms guiding galvanic replacement reactions. Advantages include the ability to (i) characterize specific structures before and after the replacement reaction through the use of substrate-based alignment markers, (ii) apply capping agents to pristine template surfaces in order to determine their influence on the replacement reaction, and (iii) apply directional external stimuli, such as polarized light or electric fields, to a well-defined ensemble of templates as they progress through the replacement reaction. Opportunities in terms of applications are derived from the fact that substrate-based nanoshells have tunable plasmonic properties which can be accessed through (i) the degree of nanostructure hollowing allowed, (ii) the formation of shapes with reduced symmetry, and (iii) the placement of the structure on a substrate offering a well-defined dielectric environment. The ability to form such structures in periodic arrays further advances this possibility by enabling the fabrication of pixelated sensing devices with plasmonic nanoshells as the active component.

4 Conclusions

Substrate-based galvanic replacement reactions carried out on heteroepitaxially formed silver templates have yielded hollow Au–Ag nanoshells. The resulting nanohut geometry is characterized by a downward facing shell with a single rectangular opening at its base. The structures are immobilized, can be placed at site-specific locations and have a LSPR peak which can be tuned to a particular frequency by varying the degree of replacement. The work, not only demonstrates the fabrication of these unique structures, but also points toward future opportunities in terms of engineering intricately shaped nanostructures using the combined capabilities of heteroepitaxial techniques and galvanic replacement reactions.

5 Methods

5.1 Silver template fabrication

The procedures for assembling templates in both the random and arrayed configurations are described in detail elsewhere [28, 29]. For both configurations the templates were assembled on epi-polished (0001)-oriented sapphire substrates (MTI). The random structures were produced through the sputter deposition (Model 681 Gatan High Resolution Ion Beam Coater) of either (i) 10 nm of antimony followed by 10 nm of silver or (ii) 5 nm of antimony followed by 2 nm of silver, depending upon whether larger (diameter < 250 nm) or smaller (diameter < 50 nm) silver templates were desired. For both cases, the heating regimen used in the self-assembly process involved placing the sample in a tube furnace (Lindberg Blue M) under an ultra high purity (UHP) argon flow (65 standard cubic centimeters per minute (sccm)) and then ramping the temperature to 750 °C in 30 min, after which it was allowed to cool to room temperature over the course of 3 h. The sample was then temperature cycled a second time to 750 °C in 30 min, a procedure which proved effective in ridding the silver structures of antimony. Nanohuts imaged using TEM were obtained using identically fabricated templates, but where the assembly process was carried out directly on Si_3N_4 support films instead of sapphire. For the arrayed configuration 70 nm of antimony, followed by 5 nm of silver, were deposited through a shadow mask. Quantifoil TEM holey carbon grids were used as shadow masks where conformal contact

was obtained by (i) applying a thin layer of acetone to the substrate, (ii) placing the grid on the substrate, and (iii) then allowing the acetone to dry. For this case, the capillary forces present during the drying process bring the two surfaces into intimate contact. After deposition, the shadow mask was peeled off the substrate, where any broken pieces of the mask remaining on the substrate were removed using ultrasonication. The silver topped antimony pedestals were twice heated to 750 °C in 12 min followed by a 3 h cool down to room temperature.

5.2 Galvanic replacement reactions

Prior to reaction, all glassware was cleaned with aqua regia. Reactions were carried out in a three-neck flask filled with an aqueous $HAuCl_4$ (Alfa Aesar) solution (10 mL) having the desired concentration (10 to 100 μM). The solution was refluxed for 10 min prior to the insertion of the substrate-based silver templates. The substrate, which was held by one corner with Teflon tweezers, was then immersed for 10 min after which it was slowly pulled out and dried in a flow of UHP argon gas.

5.3 Computer simulations

Simulations of the extinction efficiency were carried out using the DDA [44]. The calculations were performed using DDSCAT (Version 7.2) [51] where the simulated structures were first created using LAMMPS [52]. Each structure was modeled using at least 10^4 dipoles. Complex refractive indices for gold and sapphire were provided by Johnson and Christy [53], and Palik [54], respectively.

5.4 Instrumentation

SEM images were obtained in secondary electron mode using either an FEI Quanta 400 or a 600 FEG environmental scanning electron microscope (ESEM). The samples were coated with a gold–palladium film to improve imaging. TEM images were obtained using an FEI Tecnai 12T transmission electron microscope. AFM images were obtained using a Veeco Multimode atomic force microscope in tapping mode (TESP-SS AFM Probe, 2 nm radius). θ–2θ X-ray diffraction scans were measured using a Bruker D8 Discover X-ray diffractometer. Extinction spectra were measured using a Jasco UV/vis v530 spectrophotometer where the ***E***-field and propagation direction (***k***) are parallel and perpendicular to the substrate surface, respectively.

Acknowledgements

This work is funded by the National Science Foundation (NSF) CAREER Award (DMR-1053416). S. N. acknowledges Dr. Mostafa El-Sayed (Georgia Institute of Technology) for helpful discussions. The authors also acknowledge the expertise of Dr. F. Monson (Technical Director, Center for Microanalysis, Imaging, Research and Training, West Chester University) and Dr. H. Zhou (Temple University). The work has benefited from the facilities available through Temple University's Material Research Facility (MRF), the Owl's Nest high-performance computing cluster and the Penn Regional Nanotechnology Facility. K. D. G. acknowledges support received through a Temple University Graduate Student Fellowship.

Electronic Supplementary Material: Supplementary material (additional SEM images showing the (i) shape uniformity of Ag templates obtained when using a sacrificial antimony layer and (ii) Ag templates, Au–Ag nanohuts and Au–Ag nanobowls as large area periodic arrays) is available in the online version of this article at http://dx.doi.org/10.1007/s12274-013-0319-5.

References

[1] Jans, H.; Huo, Q. Gold nanoparticle-enabled biological and chemical detection and analysis. *Chem. Soc. Rev.* **2012**, *41*, 2849–2866.

[2] Atwater, H. A.; Polman, A. Plasmonics for improved photovoltaic devices. *Nat. Mater.* 2010, *9*, 205–213.

[3] Ozbay, E. Plasmonics: Merging photonics and electronics at nanoscale dimensions. *Science* **2006**, *311*, 189–193.

[4] Ma, Z.; Dai, S. Development of novel supported gold catalysts: A materials perspective. *Nano Res.* **2011**, *4*, 3–32.

[5] Xia, Y.; Xiong, Y.; Lim, B.; Skrabalak, S. E. Shape-controlled synthesis of metal nanocrystals: Simple chemistry meets complex physics? *Angew. Chem. Int. Ed.* **2009**, *48*, 60–103.

[6] Huang, X.; Neretina, S.; El-Sayed, M. A. Gold nanorods: From synthesis and properties to biological and biomedical

applications. *Adv. Mater*. **2009**, *21*, 4880–4910.

[7] Sun, Y.; Xia, Y. Shape-controlled synthesis of gold and silver nanoparticles. *Science* **2002**, *298*, 2176–2179.

[8] Sastry, M.; Swami, A.; Mandal, S.; Selvakannan, P. R. New approaches to the synthesis of anisotropic, core–shell and hollow metal nanostructures. *J. Mater. Chem.* **2005**, *15*, 3161–3174.

[9] Rycenga, M.; Cobley, C. M.; Zeng, J.; Li, W.; Moran, C. H.; Zhang, Q.; Qin, D.; Xia, Y. Controlling the synthesis and assembly of silver nanostructures for plasmonic applications. *Chem. Rev*. **2011**, *111*, 3669–3712.

[10] Xia, Y.; Halas, N. J. Shape-controlled synthesis and surface plasmonic properties of metallic nanostructures. *MRS Bull.* **2005**, *30*, 338–344.

[11] Van Dorpe, P.; Ye, J. Semishells: Versatile plasmonic nanoparticles. *ACS Nano* **2011**, *5*, 6774–6778.

[12] Prodan, E.; Radloff, C.; Halas, N. J.; Nordlander, P. A hybridization model for the plasmon response of complex nanostructures. *Science* **2003**, *302*, 419–422.

[13] Skrabalak, S. E.; Au, L.; Li, X.; Xia, Y. Facile synthesis of Ag nanocubes and Au nanocages. *Nat Protoc.* **2007**, *2*, 2182–2190.

[14] Sun, Y.; Mayers, B.; Xia, Y. Template-engaged replacement reaction: A one-step approach to the large-scale synthesis of metal nanostructures with hollow interiors. *Nano Lett.* **2002**, *2*, 481–485.

[15] Cobley, C. M.; Xia, Y. Engineering the properties of metal nanostructures via galvanic replacement reactions. *Mater. Sci. Eng. R-Rep.* **2010**, *70*, 44–62.

[16] Oldenburg, S. J.; Averitt, R. D.; Westcott, S. L.; Halas, N. J. Nanoengineering of optical resonances. *Chem. Phys. Lett.* **1998**, *288*, 243–247.

[17] Sun, Y.; Xia, Y. Increased sensitivity of surface plasmon resonance of gold nanoshells compared to that of gold solid colloids in response to environmental changes. *Anal. Chem*. **2002**, *74*, 5297–5305.

[18] Sun, Y.; Mayers, B.; Xia, Y. Metal nanostructures with hollow interiors. *Adv. Mater.* **2003**, *15*, 641–646.

[19] Hu, M.; Chen, J.; Li, Z. Y.; Au, L.; Hartland, G. V.; Li, X.; Marquez, M.; Xia, Y. Gold nanostructures: Engineering their plasmonic properties for biomedical applications. *Chem. Soc. Rev.* **2006**, *35*, 1084–1094.

[20] Fu, E.; Ramsey, S.; Chen, J.; Chinowsky, T.; Wiley, B.; Xia, Y.; Yager, P. Resonance wavelength-dependent signal of absorptive particles in surface plasmon resonance-based detection. *Sensor. Actuator. B-Chem.* **2007**, *123*, 606–613.

[21] Kim, S. W.; Kim, M.; Lee, W. Y.; Hyeon, T. Fabrication of hollow palladium spheres and their successful application to the recyclable heterogeneous catalyst for Suzuki coupling reactions. *J. Am. Chem. Soc*. **2002**, *124*, 7642–7643.

[22] Chen, H. M.; Liu, R. S.; Lo, M. Y.; Chang, S. C.; Tsai, L. D.; Peng, Y. M.; Lee, J. F. Hollow platinum spheres with nano-channels: Synthesis and enhanced catalysis for oxygen reduction. *J. Phys. Chem. C* **2008**, *112*, 7522–7526.

[23] Sabri, Y. M.; Ippolito, S. J.; Atanacio, A. J.; Bansal, V.; Bhargava, S. K. Mercury vapor sensor enhancement by nanostructured gold deposited on nickel surfaces using galvanic replacement reactions. *J. Mater. Chem.* **2012**, *22*, 21395–21404.

[24] Bansal, V.; Jani, H.; Du Plessis, J.; Coloe, P. J.; Bhargava, S. K. Galvanic replacement reaction on metal films: A one-step approach to create nanoporous surfaces for catalysis. *Adv. Mater.* **2008**, *20*, 717–723.

[25] Song, C.; Abell, J. L.; He, Y.; Murph, S. H.; Cui, Y.; Zhao, Y. Gold-modified silver nanorod arrays: Growth dynamics and improved SERS properties. *J. Mater. Chem.* **2012**, *22*, 1150–1159.

[26] Najdovski, I.; O'Mullane, A. P.; Bhargava, S. K. Electrochemical properties of galvanically replaced iron nanocubes with gold and palladium. *Electrochem. Commun.* **2010**, *12*, 1535–1538.

[27] Viyannalage, L. T.; Vasilic, R.; Dimitrov, N. Epitaxital growth of Cu on Au(111) and Ag(111) by surface limited redox replacement—An electrochemical and STM study. *J. Phys. Chem. C* **2007**, *111*, 4036–4041.

[28] Farzinpour, P.; Sundar, A.; Gilroy, K. D.; Eskin, Z. E.; Hughes, R. A.; Neretina, S. Altering the dewetting characteristics of ultrathin gold and silver films using a sacrificial antimony layer. *Nanotechnology* **2012**, *23*, 495604.

[29] Farzinpour, P.; Sundar, A.; Gilroy, K. D.; Eskin, Z. E.; Hughes, R. A.; Neretina, S. Dynamic templating: A large area processing route for the assembly of periodic arrays of sub-micrometer and nanoscale structures. *Nanoscale*, 2013, *5*, 1929–1938.

[30] Thompson, C. V. Solid-state dewetting of thin films. *Ann. Rev. Mater. Res.* **2012**, *42*, 399–434.

[31] Henry, C. R. Morphology of supported nanoparticles. *Prog. Surf. Sci.* **2005**, 80, 92–116.

[32] Sun, Y. G.; Xia, Y. N. Mechanistic study on the replacement reaction between silver nanostructures and chloroauric acid in aqueous medium. *J. Am. Chem. Soc.* **2004**, *126*, 3892–3901.

[33] Chen, J.; Wiley, B.; Li, Z.-Y.; Campbell, D.; Saeki, F.; Cang, H.; Au, L.; Lee, J.; Li, X.; Xia, Y. Gold nanocages: Engineering their structure for biomedical applications. *Adv. Mater*. **2005**, *17*, 2255–2261.

[34] Mirin, N. A.; Halas, N. J. Light-bending nanoparticles. *Nano Lett.* **2009**, *9*, 1255–1259.

[35] Zhang, Y.; Barhoumi, A.; Lassiter, J. B.; Halas, N. J. Orientation-preserving transfer and directional light scattering from Individual light-bending nanoparticles. *Nano Lett.* **2011**, *11,* 1838–1844.

[36] Ye, J.; Van Dorpe, P.; Van Roy, W.; Lodewijks, K.; De Vlaminck, I.; Maes, G.; Borghs, G. Fabrication and optical properties of gold semishells. *J. Phys. Chem. C* **2009**, *113*, 3110–3115.

[37] Ye, J.; Lagae, L.; Maes, G.; Borghs, G.; Van Dorpe, P. Symmetry breaking induced optical properties of gold open shell nanostructures. *Opt. Express* **2009**, *17*, 23765–23771.

[38] Ridelman, Y.; Singh, G.; Popovitz-Biro, R.; Wolf, S. G.; Das, S.; Klajn, R. Metallic nanobowls by galvanic replacement reaction on heterodimeric nanoparticles. *Small* **2012**, *8*, 654–660.

[39] Rao, Y.; Tao, Q.; An, M.; Rong, C.; Dong, J.; Dai, Y.; Qian, W. Novel and simple route to fabricate 2D ordered gold nanobowl arrays based on 3D colloidal crystals. *Langmuir* **2011**, *27*, 13308–13313.

[40] Li, X. L.; Zhang, Y. Z.; Shen, Z. X.; Fan, H. J. Highly-ordered arrays of particle-in-bowl plasmonic nanostructures for surface enhanced Raman scattering. *Small* **2012**, *8,* 2548–2554.

[41] Ye, J.; Van Dorpe, P.; Van Roy, W.; Borghs, G.; Maes, G. Fabrication, characterization, and optical properties of gold nanobowl submonolayer structures. *Langmuir* **2009**, *25,* 1822–1827.

[42] Shumaker-Parry, J. S.; Rochholz, H.; Kreiter, M. Fabrication of crescent-shaped optical antennas. *Adv. Mater.* **2005**, *17*, 2131–2134.

[43] Bukasov, R.; Shumaker-Parry, J. S. Highly tunable infrared extinction properties of gold nanocrescents. *Nano Lett.* **2007**, *7*, 1113–1118.

[44] Draine, B. T.; Flatau, P. J. Discrete-dipole approximation for scattering calculations. *J. Opt. Soc. Am. A* **1994**, *11*, 1491–1499.

[45] Mirin, N. A.; Ali, T. A.; Nordlander, P.; Halas, N. J. Perforated semishells: Far-field directional control and optical frequency magnetic response. *ACS Nano* **2010**, *4*, 2701–2712.

[46] Wan, D.; Xia, X.; Wang, Y.; Xia, Y. Robust synthesis of gold cubic nanoframes through a combination of galvanic replacement, gold deposition, and silver dealloying. *Small*, in press, DOI: 10.1002/smll.201203233.

[47] Vitos, L.; Ruban, A. V.; Skriver, H. L.; Kollar, J. The surface energy of metals. *Surf. Sci.* **1998**, *411*, 186–202.

[48] Graoui, H.; Giorgio, S.; Henry, C. R. Effect of the interface structure on the high-temperature morphology of supported metal clusters. *Philos. Mag. B* **2001**, *81*, 1649–1658.

[49] Devenyi, G. A.; Li, J. F.; Hughes, R. A.; Shi, A.-C.; Mascher, P.; Preston, J. S. Epitaxially driven formation of intricate supported gold nanostructures on a lattice-matched oxide substrate. *Nano Lett.* **2009**, *9*, 4258–4263.

[50] Silly, F.; Castell, M. R. Selecting the shape of supported metal nanocrystals: Pd huts, hexagons, or pyramids on $SrTiO_3$(001). *Phys. Rev. Lett.* **2005**, *4,* 046103.

[51] Draine, B. T.; Flatau, P. J. *User Guide to the Discrete Dipole Approximation Code DDSCAT 7.2* [online]. http://arXiv.org/abs/1202.3424 (accessed 2012).

[52] Plimpton, S. Fast parallel algorithms for short-range molecular-dynamics. *J. Comput. Phys.* **1995**, *117*, 1–19.

[53 Johnson, P. B.; Christy, R. W. Optical constants of the nobel metals. *Phys. Rev. B* **1972**, *6*, 4370–4379.

[54] Palik, E. D. *Handbook of Optical Constants of Solids*; Academic Press: San Diego, 1998.